Gaussian curvature elasticity determined from global shape transformations and local stress distributions

Hu, Mingyang; de Jong, Djurre H.; Marrink, Siewert J.; Deserno, Markus

Published in:
Faraday Discussions

DOI:
10.1039/c2fd20087b

Publication date:
2013

Gaussian curvature elasticity determined from global shape transformations and local stress distributions: a comparative study using the MARTINI model

Mingyang Hu,[a] Djurre H. de Jong,[b] Siewert J. Marrink[b] and Markus Deserno*[a]

Received 28th April 2012, Accepted 28th May 2012
DOI: 10.1039/c2fd20087b

We calculate the Gaussian curvature modulus $\bar{\kappa}$ of a systematically coarse-grained (CG) one-component lipid membrane by applying the method recently proposed by Hu *et al.* [*Biophys. J.*, 2012, **102**, 1403] to the MARTINI representation of 1,2-dimyristoyl-*sn*-glycero-3-phosphocholine (DMPC). We find the value $\bar{\kappa}/\kappa = -1.04 \pm 0.03$ for the elastic ratio between the Gaussian and the mean curvature modulus and deduce $\bar{\kappa}_\mathrm{m}/\kappa_\mathrm{m} \approx -0.98 \pm 0.09$ for the monolayer elastic ratio, where the latter is based on plausible assumptions for the distance z_0 of the monolayer neutral surface from the bilayer midplane and the spontaneous lipid curvature $K_{0\mathrm{m}}$. By also analyzing the lateral stress profile $\sigma_0(z)$ of our system, two other lipid types and pertinent data from the literature, we show that determining $K_{0\mathrm{m}}$ and $\bar{\kappa}$ through the first and second moment of $\sigma_0(z)$ gives rise to physically implausible values for these observables. This discrepancy, which we previously observed for a much simpler CG model, suggests that the moment conditions derived from simple continuum assumptions miss the effect of physically important correlations in the lipid bilayer.

1 Introduction

Self-assembled from their lipid constituents, bilayer membranes provide a continuous barrier to enclose living cells from their environment and form internal compartments with various functionalities in eukaryotic cells.[1] On length scales that exceed their thickness by a very modest factor, the energetics of membranes follow a curvature–elastic continuum theory, developed in its current standard form 40 years ago by Wolfgang Helfrich.[2] Representing a piece of lipid bilayer as an idealized two-dimensional surface patch $\mathcal{P}$ with boundary $\partial\mathcal{P}$, the theory states that the (free) energy of that membrane can be written as an area integral over $\mathcal{P}$ of an energy density that is at most quadratic in the local principal curvatures c_1 and c_2, plus a line integral over $\partial\mathcal{P}$:[2,3]

$$E[\mathcal{P}] = \int_{\mathcal{P}} \mathrm{d}A \left\{ \frac{1}{2}\kappa(K - K_0)^2 + \bar{\kappa}K_\mathrm{G} \right\} + \oint_{\partial\mathcal{P}} \mathrm{d}s\gamma. \qquad (1)$$

[a]*Carnegie Mellon University, 5000 Forbes Avenue, Pittsburgh, PA 15213, USA. E-mail: deserno@andrew.cmu.edu*
[b]*Groningen Biomolecular Sciences and Biotechnology Institute & Zernike Institute for Advanced Materials, University of Groningen, Nijenborgh 7, 9747 AG Groningen, The Netherlands*

The two independent variables, $K = c_1 + c_2$ and $K_G = c_1c_2$, are the total and Gaussian curvature of the surface, respectively. Four empirical material parameters suffice to describe the physics: the bending modulus κ, the Gaussian curvature modulus $\bar{\kappa}$, the spontaneous membrane curvature K_0, and the edge tension γ.

Following a significant amount of work conducted since the early 1970s, κ, K_0 and γ are now fairly well understood and often known with good accuracy for common experimental systems. For instance, the bending modulus κ can be experimentally measured by flicker spectroscopy,[4–9] X-ray scattering,[10–13] or micro-pipette aspiration[14–16] methods, or it may be determined by undulation mode analysis[17–26] or tensile force measurements of tethers[27–29] in computer simulations. The edge tension can be obtained by studying pores, both in experiments[30–33] and in simulations.[20–24] The spontaneous membrane curvature K_0 vanishes for symmetric bilayers (a situation we will also restrict to in this work). However, due to the subtle nature of the Gaussian curvature K_G, whose surface integral remains constant if there is no change in topology or boundary,[34,35] it is difficult to obtain a signal which is sensitive to the Gaussian curvature modulus $\bar{\kappa}$, leaving the remaining one of the four material parameters in the Helfrich theory less understood. While indeed its value does not matter when neither topology nor boundary change, a number of important biological processes depend on the Gaussian term, such as those occurring during membrane remodelling, endo- and exo-cytosis, cell division and neurotransmission, *etc.*[1] Being able to determine the Gaussian curvature modulus would help us to better understand these cases, including the question whether nature has chosen to adjust the value of $\bar{\kappa}$ to tune the energetics of these events.

In a recent study,[36] we proposed a novel method to determine the Gaussian curvature modulus $\bar{\kappa}$ using molecular dynamic (MD) simulations. Through monitoring the interplay between the curvature-elastic energy and the edge energy during the closing-up process of open bilayer patches, $\bar{\kappa}$ could be extracted with a statistical error of just a few percent. The theoretical background of this method will be briefly reviewed in the following section. To demonstrate the applicability of our method, we measured the value of $\bar{\kappa}$ for several bilayers that differ in bending rigidity κ and lipid spontaneous curvature K_{0m}, using a generic top-down membrane model,[23,24] in which each lipid is represented by three linearly connected beads. The results are in line with the sparsely available experimental measurements,[37–43] as well as some simulation studies.[44,45] In addition, the required computing resources turned out to be very modest, which suggested the possibility to apply this method to other more chemically specific coarse-grained (CG) lipid models and obtain $\bar{\kappa}$ values for common lipid systems, such as 1,2-dipalmitoyl-*sn*-glycero-3-phosphocholine (DPPC) and 1,2-dimyristoyl-*sn*-glycero-3-phosphocholine (DMPC).

In the same study, we also questioned the applicability of an alternative way to determine $\bar{\kappa}$, namely through the moments of the lateral stress profile $\sigma_0(z)$. With the generic CG model we studied in ref. 36, the $\sigma_0(z)$-deduced lipid spontaneous curvature K_{0m} and the Gaussian curvature modulus $\bar{\kappa}$ were neither consistent with the results from the patch-closure method, nor with some well-educated expectations.[41] At first glance, the simplicity of the generic lipid model, the missing local correlations and its unphysical stress profile may be blamed as the culprit. Yet, in the absence of further tests, it remained unclear whether lipid models with a higher resolution could indeed produce more physical results. This has important practical implications, because, if one could obtain $\bar{\kappa}$ *via* the stress profile method, this would be both straightforward and computationally (relatively) inexpensive. Besides, such a test could potentially teach us how much chemical specificity would be needed to yield stress profiles that quantitatively link to large scale bilayer elastic properties.

In the present paper, after a brief review of the pertinent theoretical background, we will first apply the patch-closure method introduced in ref. 36 to the widely used MARTINI[21,46] lipid model. This model is not merely a generic representation of amphiphilic entities that assemble into bilayers (like the Cooke model we used previously), but has instead been systematically and quantitatively constructed to

describe specific lipids. We chose to pick the case of DMPC and will therefore be able to predict – by combining systematic coarse-graining with our patch-closure measurement – the value of the Gaussian curvature rigidity $\bar{\kappa}$ and the elastic ratio $\bar{\kappa}/\kappa$ for an actual chemically specific lipid membrane. We will then test whether the stress profile, which for MARTINI-DMPC is much closer to physical expectations than for the Cooke model, constitutes a reliable predictor of the Gaussian modulus.

The MARTINI model is chosen for three different reasons:

1. It has proven to be a useful tool for a broad spectrum of biophysical problems, *e.g.* the phase behavior of lipid mixtures,[47] membrane fusion,[48,49] membrane rafts and domains[50,51] and mechano-sensitive protein gates.[52]

2. Many relevant properties of the model, such as the bending modulus κ and the area per lipid A_L have already been analyzed carefully,[53] allowing us to use these results when determining the Gaussian curvature modulus $\bar{\kappa}$.

3. In contrast to the implicit-solvent Cooke model used in the original demonstration, the MARTINI model represents water explicitly (in a CG fashion). We will show that this does not cause the basic strategy to fail.

Of course, the patch-closure method would also work for other lipid models around the same resolution, even though it might still be a bit too ambitious to apply it to an all-atom simulation.

2 Theory

In this section, we will briefly review the theoretical framework of both the patch-closure and the stress profile method for determining the Gaussian curvature modulus.

2.1 Patch-closure method

Consider a circular membrane patch of area A closing up into a vesicle in such a way that its shape is always an axisymmetric cap of a sphere of curvature radius c^{-1}. Using the Hamiltonian from eqn (1), simple geometry shows that the energy can be expressed as[36,54]

$$\frac{\Delta E(x,\xi)}{4\pi(2\kappa+\bar{\kappa})} = \Delta\tilde{E}(x,\xi) = x + \xi\left[\sqrt{1-x}-1\right]. \tag{2}$$

Here, $\Delta\tilde{E}(x, \xi)$ is the energy difference between a *curved* patch and its flat counterpart, scaled by the bending energy of a closed spherical vesicle, and

$$x = (Rc)^2, \qquad \xi = \frac{\gamma R}{2\kappa+\bar{\kappa}}, \qquad \text{and} \qquad R = \sqrt{\frac{A}{4\pi}}. \tag{3}$$

The dimensionless "reaction coordinate" x changes between 0 (flat patch) and 1 (complete vesicle of radius R). All material parameters, κ, $\bar{\kappa}$, edge tension γ, and patch area A combine into a *single* parameter ξ, which fully determines the functional form of the energy. When $\xi < 1$, the flat state is globally stable. Beyond $\xi = 1$ the vesicle state becomes more stable, yet is separated from the flat state by an energy barrier of $\Delta\tilde{E}^* = (1 - \xi/2)^2$ situated at $x^* = 1 - (\xi/2)^2$, as long as $1 < \xi < 2$. For $\xi > 2$, a flat disk will immediately close into a vesicle without first having to surmount a barrier.†

If we can determine the value of ξ in eqn (3), the Gaussian curvature modulus $\bar{\kappa}$ can be extracted, because all the other parameters in the definition of ξ can be

† Note that a two-dimensional equivalent of the Young–Laplace law demands that lipids in a flat circular patch of radius r feel a compressive stress $\Sigma_\gamma = \gamma/r$. This stress is on the order of a few mN m^{-1} and thus not small. However, a patch that is buckled into the third dimension has most of this stress relieved and it is these patches that are most relevant, as they are at the top of the energy barrier.

determined by independent simulation methods. Hence, the parameter ξ uniquely determines the form of the energy barrier $\Delta\tilde{E}(x, \xi)$, and the latter can be both precisely and easily measured by the following sequence of steps:

1. Choose systems with moderate sizes such that $1 < \xi < 2$; in other words, systems for which an energy barrier exists. (This poses certain restrictions on the membrane's material parameters, as discussed in the supplementary information of ref. 36.)

2. Prepare lipid bilayers in pre-curved initial states with different x-values along the barrier.

3. Measure the probability $P_{\mathrm{close}}(x)$ of such patches closing up into the vesicle state. This so-called splitting probability[55] can be analytically predicted from $\Delta\tilde{E}(x, \xi)$ and thus knowing P means knowing $\Delta\tilde{E}$ and thus ξ.

Two main concerns about this method are noteworthy. Firstly, the shape of the membrane is required to remain in its spherical cap ground state, so that the undulation contribution to the free energy can be neglected. The bilayer should therefore not be too large (which limits the combination of $(\kappa, \bar{\kappa}, \gamma)$ for which the technique can profitably be employed). Secondly, the existence of solvent will not affect the applicability of this method. As shown by Noguchi and Gompper,[56] hydrodynamic interactions speed up the dynamics of vesiculation, but will not affect the probability of closure. Although the hydrodynamics might become complex when a membrane is about to close up, it is safe to terminate the simulation shortly before that complication steps in because the gradient of $\Delta\tilde{E}(x,\xi)$ close to $x = 1$ tends to be big enough such that the probability of avoiding final closure is small. In addition, hydrodynamics makes the to-be vesicles more spherical[56] and thus helps them to closely follow the assumed pathway.

Recently, Shinoda *et al.*[57] have proposed a related simulation protocol in which a closed vesicle is pried open by pushing a cone into it. These authors wanted to determine the free energy needed to create a pore and open up the vesicle, and the model just discussed is one way of analyzing their simulations. They found, however, that it does not work in their case and proposed that the model neglects contributions to the free energy, specifically the repartitioning of lipids between the leaflets. We wish to emphasize that eqn (2) implicitly assumes a quasi-instantaneous equilibration of lipids between the inner and outer leaflet of the bilayer as it contains no contribution due to area difference elasticity. While this might be questionable for small pores of almost closed vesicles, the important "signal" in our simulation protocol emerges from partially open vesicles, which are half-way between flat and closed (in fact, $x^* \approx 0.5$ in the case studied in this paper, as the inset of Fig. 3 shows). We therefore believe that such complications will not matter in our case and that the theoretical description provided above is appropriate (as we have previously[36] found for a different lipid model).

2.2 Stress profile method

In this section, we briefly address two issues: first, we present a simple geometric derivation of the conditions relating the elastic parameters to the moments of the stress profile; and second, we show that thermal undulations of the bilayer, which smear out the stress profile, nevertheless do not affect these moments.

2.2.1 The moment conditions. Various arguments have been put forward in the literature to link the phenomenological elastic parameters in Helfrich theory to properties of the lateral stress profile across a real membrane of finite thickness.[58–63] In its most basic version, such a relation follows from a mapping between the energy of a deformed thin continuum elastic sheet to the effective Helfrich theory of an infinitely thin curvature elastic surface. Let us briefly outline the argument.

A basic result in differential geometry states that when we displace a surface by a fixed distance z along the local normal, the new "parallel surface" area element $\mathrm{d}A'(z)$ and the total curvature $K'(z)$ can be expressed in terms of the area element $\mathrm{d}A$ and the total curvature K of the original surface as

$$dA'(z) = dA\,[1 + Kz + K_G z^2 + O(z^3)]\,, \tag{4a}$$

$$K'(z) = K\,[1 + (2K_G/K - K)z + O(z^2)]\,. \tag{4b}$$

Furthermore, assuming a linear stress–strain relationship, the lateral stress profile $\sigma(z)$ of a *curved* bilayer can plausibly be written as

$$\sigma(z) = \sigma_0(z) + \varepsilon(z)Y(z), \tag{5}$$

where $\sigma_0(z)$ is the stress profile of the *uncurved* patch, $\varepsilon(z)$ is the curvature-induced area strain and $Y(z)$ is a local Young modulus (which we might not know, but which turns out to be irrelevant for the present purpose). Here, *positive* lateral stress (*i.e. negative* lateral pressure) means the surface is under tension. If one picks the reference position at the neutral surface z_0 inside the material, where neither compression nor stretching happens when the sheet is bent, then eqn (4a) and (5) together lead to

$$\varepsilon(z) = dA'(z)/dA - 1 = K(z - z_0) + K_G(z - z_0)^2 + O((z - z_0)^3)\,. \tag{6}$$

Integrating the stress across one monolayer allows the deformation energy per area to be written as

$$e_m = \int_{-z_0}^{\infty} dz \int_0^{\varepsilon(z)} d\varepsilon' \sigma(\varepsilon'). \tag{7}$$

The total monolayer curvature energy E_m equals the surface integral of e_m over the neutral surface (henceforth, monolayer observables will be labeled with a subscript "m"). Thus, by matching the prefactors of the curvature terms (after shifting the reference plane back to the mid-plane of the bilayer), one arrives at the relationship between the total bilayer surface tension Σ, the lipid curvature K_{0m}, the monolayer Gaussian curvature modulus $\bar{\kappa}_m$ and the stress profile $\sigma_0(z)$:

$$\frac{1}{2}\Sigma = \int_0^{\infty} dz\ \sigma_0(z), \tag{8a}$$

$$-\kappa_m K_{0m} = \int_0^{\infty} dz\ \sigma_0(z)(z - z_0), \tag{8b}$$

$$\bar{\kappa}_m = \int_0^{\infty} dz\ \sigma_0(z)(z - z_0)^2. \tag{8c}$$

Note that, in the case of zero surface tension, $\Sigma = \int dz\ \sigma_0(z) = 0$, eqn (8b) is in effect independent of z_0.

It also straightforwardly follows that the Gaussian curvature modulus $\bar{\kappa}$ for the bilayer can be simply obtained by extending the lower integration range in eqn (8c) to minus infinity and setting z_0 to zero:

$$\bar{\kappa} = \int_{-\infty}^{\infty} dz\ \sigma_0(z) z^2. \tag{9}$$

Thus, $\bar{\kappa}$ is identified as the second moment of the lateral stress profile of a flat membrane. Furthermore, as a natural consequence of eqn (8) and (9), the bilayer and monolayer Gaussian moduli are related by

$$\bar{\kappa} = 2\left(\bar{\kappa}_{\mathrm{m}} - 2K_{0\mathrm{m}}z_0\kappa_{\mathrm{m}} + \frac{1}{2}z_0^2\Sigma\right), \tag{10}$$

where the third term of course vanishes at zero surface tension.

2.2.2 Impact of bilayer undulations on stress profile moments. Due to the unavoidable bilayer undulations, the stress profile $\sigma_0(z)$ is invariably smeared out. Let us write its measured value as the convolution of some idealized perfectly flat membrane stress profile, $\sigma_0^*(z)$, with a function $w(z)$ describing the probability density of vertical bilayer displacements:

$$\sigma_0(z) = \int_{-\infty}^{\infty} \mathrm{d}z'\sigma_0^*(z')w(z-z'), \tag{11}$$

and thus the n^{th} moment of the actual stress profile can be expressed as

$$[z^n]_{\sigma_0} \equiv \int_{-\infty}^{\infty} \mathrm{d}z\ z^n\sigma_0(z) = \int_{-\infty}^{\infty} \mathrm{d}z'\sigma_0^*(z') \int_{-\infty}^{\infty} \mathrm{d}z\ (z+z')^n w(z). \tag{12}$$

Notice that as long as $w(z)$ is normalized and symmetric around $z = 0$ and the bilayer is under zero tension, the zeroth, first and second moment are in fact *independent* of $w(z)$. Hence, while the actual profile $\sigma_0(z)$ will look different for bigger membranes which fluctuate more (it will have broader peaks of lower height), the value of $\bar{\kappa}$ deduced from the second moment through eqn (9) is not affected. For a symmetric bilayer the lowest moment that notices the fluctuations is the fourth one: $[z^4]_{\sigma_0} = [z^4]_{\sigma_0^*} + 6\langle z^2\rangle_w [z^2]_{\sigma_0^*}$.

Unfortunately, the same independence of $w(z)$ is not true for the monolayer moments, since now the function $w(z)$ will not end up being integrated over its entire range. Instead, we find

$$[(z-z_0)^n]_{\sigma_0,\mathrm{m}} = \int_{-\infty}^{\infty} \mathrm{d}z'\sigma_0^*(z') \int_{-z'}^{\infty} \mathrm{d}z\ (z+z'-z_0)^n w(z). \tag{13}$$

If, for simplicity, we assume that $w(z)$ is a centered Gaussian with variance δ^2, then we can, for instance, rewrite the first monolayer moment as

$$[z-z_0]_{\sigma_0,\mathrm{m}} = \int_{-\infty}^{\infty} \mathrm{d}z'\sigma_0^*(z')\, W_\delta(z', z_0) \tag{14a}$$

with

$$W_\delta(z, z_0) = \frac{\delta}{\sqrt{2\pi}}\mathrm{e}^{-z^2/2\delta^2} + \frac{z-z_0}{2}\left(1 + \mathrm{erf}\frac{z}{\sqrt{2}\delta}\right). \tag{14b}$$

It is easy to check that in the limit $\delta/z_0 \to 0$ the function $W_\delta(z,z_0)$ converges against $(z - z_0)\Theta(z)$, where $\Theta(z)$ is the Heaviside step function. Hence, if the membrane undulations are small compared to the distance of the neutral surface from the bilayer midplane, the fluctuation-smeared moments are approximately independent of the smearing. This holds also for the second moment. For a square membrane at zero tension, with a side length of L and bending modulus κ, it is easy to see that $\delta^2 \approx k_{\mathrm{B}}TL^2/16\pi^3\kappa$, which in our case ($\kappa \approx 40k_{\mathrm{B}}T$) leads to $\delta \approx L/140$. Hence, if we demand $\delta/z_0 < 0.1$ and take $z_0 = 1.25$nm, undulations will only matter once the membrane side length L exceeds 17.5nm, which at an area per lipid of 0.6nm^2

corresponds to about 1000 lipids. This is bigger than the biggest membrane for which we have calculated a stress profile in this work.

3 Methods

3.1 The MARTINI model

All simulations in the paper use version 2.0 of the MARTINI CG force field (FF).[46] In this FF, every four heavy atoms in a molecule are mapped to one of the basic building blocks, depending on their polarity, net charge and the ability to form hydrogen bonds. These building blocks have been parameterized to reproduce most of the thermodynamics correctly, especially the partitioning free energy between different environments, such as between an aqueous solution and oil. According to their chemical structure, the building blocks are connected with standard bonded interactions, *i.e.* harmonic, angular and dihedral potentials. The non-bonded interactions consist of short-ranged shifted Lennard–Jones (LJ) potentials. In addition, groups with explicit charges interact *via* shifted Coulomb interactions. LJ and Coulomb potentials and forces approach zero smoothly at the cutoffs. Details about the definition of the basic building blocks, the methods of parametrization and the interaction parameters, can be found in the original papers.[21,46] The MARTINI FF is currently available for common lipids, peptides, sterols and other systems. The DMPC lipids simulated in this study are composed of 10 beads: one choline (+1 charge), one phosphate (−1 charge), two glycerol beads and three beads for each of the two tails. Some important material properties of MARTINI DMPC, such as the area per lipid and bending modulus κ, were carefully determined in a recent study.[53]

3.2 Simulation details

MD simulations were conducted with GROMACS 4.x simulation packages.[64] The leap-frog integration method[65] was adopted with an integration time step of 20 fs and the neighbor list (with a 1.2nm cutoff) was updated every 10 time steps. Standard cutoffs of 1.2 nm in the MARTINI FF for LJ and Coulomb interactions were used. The relative dielectric constant was chosen as $\varepsilon_r = 15$. To set the temperature, lipids and solvent molecules were separately coupled to a Berendsen thermostat[66] with a time constant $\tau_T = 2$ ps. Simulated systems were also coupled to a Berendsen barostat[66] with time constant $\tau_p = 3$ps and (isothermal) compressibility $\kappa_T = 3 \times 10^{-5}$ Pa^{-1}. For the patch-closure simulations, isotropic pressure-coupling was used, while in the stress profile simulations the box lengths in lateral (xy) directions were allowed to adjust independently (but isotropically) from the normal (z) direction.

3.3 System setup

3.3.1 Patch-closure simulations. Curved membrane caps with 1200 DMPC lipids were solvated and put into various spherical constraining potential fields for 10 ns. During this time period, the patch was sandwiched (but not squeezed) by the field in such a way that the membrane curvature was essentially held constant at a specific chosen value, while the area per lipid and the open edge at the boundary could relax because of lateral lipid diffusion. This constraining field was implemented using the Mean Field Force Approximation boundary (MFFA) approach[67] and only interacts with the lipids, not the water. The radial distribution function of the terminal beads in the lipid tails was calculated with respect to the center of the constraining field; their peak position gives a more accurate indication of the membrane curvatures to be used in the later analysis.

The systems with various curvatures are then put through a short energy minimization process before serving as the starting configurations for the closing/opening

simulations. For each initial configuration, 60 independent simulations were run to get the closing-up probabilities. A relative shape anisotropy index κ_s^2, defined as a combination of the eigenvalues of the gyration tensor,[68] was used to monitor the progress of each simulation. If $\kappa_s^2 > 0.21$, then a bilayer is labeled as flat, while $\kappa_s^2 < 0.008$ means a closed vesicle is about to form.‡

In both cases, the simulation was stopped and the final state of each simulation was recorded. The probability of membrane closure at each initial curvature (and thus initial x) was calculated, the error of which was estimated from Binomial statistics.

Lastly, the parameter ξ was obtained from fitting the measured splitting probability to a corresponding analytical expression.[55] To estimate the error bar of ξ, Monte Carlo (MC) resampling over the original data set was repeated 1000 times. Fitting results from the resampled sets provided the mean and standard deviation of ξ. With γ, A and κ determined from independent simulations, $\bar{\kappa}$ was then calculated from eqn (3), with its error from the error propagation relations with other parameters.

3.3.2 Stress profile simulations. Flat bilayers were simulated under zero lateral mechanical tension. This is much more straightforward than the simulations using the patch-closure method, but the analysis following the simulations is more subtle.

For a system of N DMPC lipids, exactly $N/2$ of them were put into each monolayer, making sure that the two monolayers are symmetric. After equilibration, trajectories were first generated with the standard version of GROMACS 4.5 and then fed into a customized version of GROMACS 4.0.2[69] for a "re-run" to calculate the 3D pressure fields. In this package, the local pressure tensor contains a kinetic and a virial contribution.[69]

$$p_V^{\alpha\beta} = \frac{1}{V}\sum_{i\in V} m_i v_i^\alpha v_i^\beta + \sum_n \frac{1}{nV}\sum_{\langle j\rangle}\sum_{\langle k,l\rangle}\left(\nabla_{j_k}^\alpha U^n - \nabla_{j_l}^\alpha U^n\right)\frac{r_{j_l j_k}^\beta}{N} \times \sum_{\lambda=0}^{N} f_V\left(\mathbf{r}_{j_l} + \frac{\lambda}{N}\mathbf{r}_{j_l j_k}\right), \tag{15}$$

where $p_V^{\alpha\beta}$ is the $\alpha\beta$ component of the average pressure tensor for the volume V; m_i, $\mathbf{v}_i$ and $\mathbf{r}_i$ denote the mass, velocity and position of particle i, respectively. $\langle j\rangle$ means a summation over all n clusters in the system; $\langle k,l\rangle$ go over all pairs of particles within a given cluster. The Irving–Kirkwood contour is discretized into the position-dependent function $f_V(\mathbf{r}) = 1$, if $\mathbf{r} \in V$ and zero otherwise. For the details and technicalities, see Ollila *et al.*[69]

The resulting 3D pressure field was averaged over all bins within the same slices, which are parallel to the bilayer (xy) plane, giving the pressure tensor $P^{\alpha\beta}(z)$ along the normal direction. The standard error was also calculated during the averaging. The stress profile is obtained as $\sigma_0(z) = -\frac{1}{2}[P^{xx}(z) + P^{yy}(z)] + P^{zz}(z)$, with the same sign convention as in eqn (5). Two different bin sizes of 0.05 and 0.10 nm were tested, showing no difference in the results. The smaller bin size of 0.05 nm was used for all of the results presented in this paper. For reasons of mechanical stability, $P^{zz}(z)$ must be constant, which is one further useful check.

Due to the big fluctuations of instantaneous pressure (normally on the order of several hundred bar), all simulations have at least 2 μs equilibration time, followed by a production run of 1 μs. The time intervals between two consecutive frames in a trajectory were 10 ps. The error was determined from averaging within each z-slice. The same type of error analysis was applied to all stress profile simulations described in this paper. For the calculation of curvature-elastic properties *via* eqn (8) and (9), the numerical integration was done as follows: each successive four data points were fit to a cubic polynomial and integrated.[70] Before that, the stress profiles were symmetrized, but not smoothed.

‡ For reference, $\kappa_s^2 = 0$ indicates an ideal closed sphere, while $\kappa_s^2 = \frac{1}{4}$ holds for an infinitely thin, flat and circular disk.

4 Results

4.1 Patch-closure method

To obtain the probabilities of patch-closure, $P_{\text{close}}(x)$, six sets of simulations with various initial curvatures were conducted. Each set contains 60 independent repeats. The probabilities $\{P_{\text{close}}(x_i)\}_{i=1\text{–}6}$ were then fit to get ξ, as illustrated in the inset of Fig. 3. The results are listed in Table 1, together with all other parameters required to determine $\bar{\kappa}$: the area per lipid $A_L = 0.595$ nm^2 was measured with a statistical error that is much less than 0.1%. This result is 2% smaller than the experimental value of 0.606 ± 0.005 nm^2.[71] The edge tension $\gamma = 40.49 \pm 0.34$ pN was measured by simulating bilayer ribbons with open edges,[72–75] which is consistent with the value of 50 ± 10 pN previously measured with MARTINI-DPPC lipids by studying pores[21] and is compatible with the atomistic simulations of DMPC by Jiang *et al.*,[74] who find a value of $\gamma = 10$–30 pN by studying a ribbon. Experimentally, the edge tension is a challenging quantity to determine, since it involves studying pores under controlled conditions. For instance, Chernomordik *et al.*[76] found a value of 9 pN for natural lecithin and Zhelev and Needham[31] found 9 pN for SOPC and 30 pN for SOPC with 50 mol% added cholesterol. These values are of the same order of magnitude as our measured value for MARTINI-DMPC, but somewhat smaller. This might be because DMPC is fully saturated, or because MARTINI does not get the value of γ completely right. In any case, the edge tension is a highly subtle observable even experimentally, maybe best illustrated by the fact that Karatekin *et al.*[33] found a value of 9 pN or 21 pN for DOPC, depending on whether the lipid had been supplied by Sigma or Avanti Polar Lipids, respectively.

By applying the method of Brandt *et al.*,[53] the bending modulus κ was determined through an analysis of the undulation spectrum of a bilayer under zero tension. From a set of four independent 2 μs simulations of 8192 DMPC lipids, $\kappa = (16.6 \pm 0.5) \times 10^{-20}$ J was measured. This value is about 10% larger than the original published result[53] of 15×10^{-20} J and also somewhat larger than the upper bound of experimental results $(5\text{–}15) \times 10^{-20}$ J.[63] However, comparable results of 13.4×10^{-20} J for DPPC[77] and $(7\text{–}20) \times 10^{-20}$ J for DOPC[29] have recently been reported using area spectra analysis and tether pulling methods, respectively. How an uncertainty in the bending rigidity affects our analysis will be revisited in Sec. 5. The reduced parameter ξ in eqn (2) could be pinpointed with about 0.3% relative error to $\xi = 1.359 \pm 0.004$.

Inserting the measured values of A, γ and ξ into the definition of ξ, one finds $2\kappa + \bar{\kappa} = \gamma R/\xi = (15.9 \pm 0.1) \times 10^{-20}$ J, with an error of less than 1%. Together with the value $\kappa = (16.6 \pm 0.5) \times 10^{-20}$ J this leads to a prediction for the elastic ratio $\bar{\kappa}/\kappa$ for DMPC of -1.04 ± 0.03. Although the bilayer elastic ratio of DMPC is not available from experiments, this result is in concordance with our previous simulation study,[36] in which $\bar{\kappa}/\kappa \sim -1$ for lipids with very slight positive curvatures.

The transition state has a curvature radius of $1/c^* = R/\sqrt{1-(\xi/2)^2}$. With $R \approx 5.33$nm and $\xi \approx 1.359$, we find $1/c^* \approx 7.3$nm, which is about twice the bilayer thickness. This is indeed highly curved, but based on our experience with simpler

Table 1 Measurements of the material properties of MARTINI-DMPC at $T = 300$ K[a]

A_L [nm^2]	γ [pN]	ξ	κ [10^{-20} J]	$\bar{\kappa}$ [10^{-20} J]	$\bar{\kappa}/\kappa$
0.595	40.49 ± 0.34	1.359 ± 0.004	16.6 ± 0.5	-17.3 ± 1.0	-1.04 ± 0.03

[a] A_L is the area per lipid molecule, with an error much less than 0.1%; γ is the excess free energy per length of an open edge; ξ is the parameter in the free energy from eqn (2); κ is the bending modulus; $\bar{\kappa}$ is the Gaussian curvature modulus. The number of lipids in the system is 1200, which gives a radius of $R = 5.33$nm for the final vesicles.

models[36] we expect the anharmonic curvature corrections to still be small. Moreover, the energy barrier is found to be $4\pi(2\kappa + \bar{\kappa})[1 - (\xi/2)^2] \approx 50 k_B T$, partially explaining why the crossover curve for $P(x)$ (see inset in Fig. 3) is so sharply defined and why we need not worry about patch undulations. Both points show that the requirements necessary for the patch-closure method to work indeed hold.

If one is willing to make some plausible assumptions about K_{0m} and z_0, the monolayer elastic ratio can be roughly estimated using eqn (10). Experimentally, K_{0m} of DMPC lipids is expected to be positive.[78] Together with the fact that DMPC lipids self-aggregate into a planar bilayer, K_{0m} is likely to be in the range of (0…0.05) nm^{-1}. The value of z_0, *i.e.* the position of the neutral surface, is debatable; however, it is generally believed to be located around the hydrophilic/hydrophobic interface.[41] The thickness of a DMPC bilayer is 3.53 nm,[71] so for a rough estimate one may take $z_0 \sim 1.25$ nm, which is about 70% of the monolayer thickness away from the bilayer center. Thus, $2K_{0m}z_0$ is approximately 0–0.125. Inserting this into eqn (10) leads us to estimate that $\bar{\kappa}_m/\kappa_m \approx -0.92$ to -1.04 ± 0.03 or -0.98 ± 0.09.

4.2 Stress profile method

Examples of the calculated stress profiles can be found in Fig. 1 and 2. They all share the following general features: at the center of the bilayer the compressed hydrocarbon chains repel and thus exhibit a negative stress. At the hydrophilic/hydrophobic interface (*e.g.* around $z \simeq 1.25$ nm in Fig. 1), a strong positive stress of several hundreds of bar is measured. Then, the headgroup region becomes repulsive again, showing a negative stress which gradually vanishes into the bulk of water. These features are qualitatively in line with previously calculated profiles of MARTINI-DPPC[46] (as shown in Fig. 2) and other studies of membrane stress profiles.[79–83]

Our results for curvature–elastic properties deduced *via* the stress profile are summarized in Table 2. All three types of studied lipids (DMPC, DPPC and DOPC) show negative spontaneous curvatures, which follow the right order but are too strong compared to expectations or experimental results (slightly positive for DMPC,[78] around 0 for DPPC[46] and -0.05 to -0.07nm^{-1} for DOPC[84]). More importantly, the bilayer elastic ratios of DPPC and DOPC calculated from the stress profiles turn out to be *positive*. Although this is a natural result of the strongly

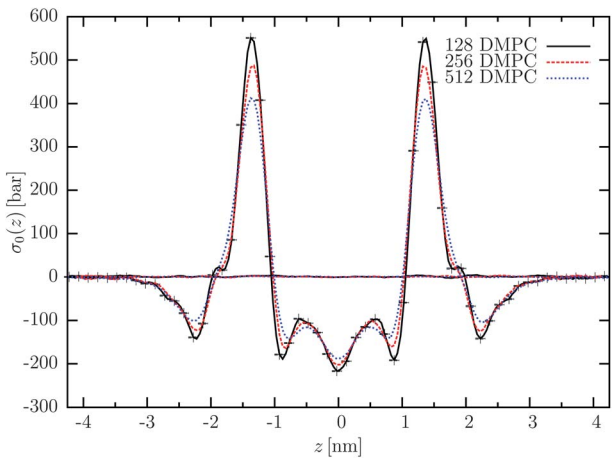

Fig. 1 The lateral stress profiles of DMPC bilayers with 128 (solid, black), 256 (dashed, red) and 512 (dotted, blue) lipids, placed such that $z = 0$ is the bilayer center. The normal component of the pressure tensor is also shown, which stays constant within the error bars. In order to show the size of the error bars, only one out of three data points were plotted for the system with 128 lipids.

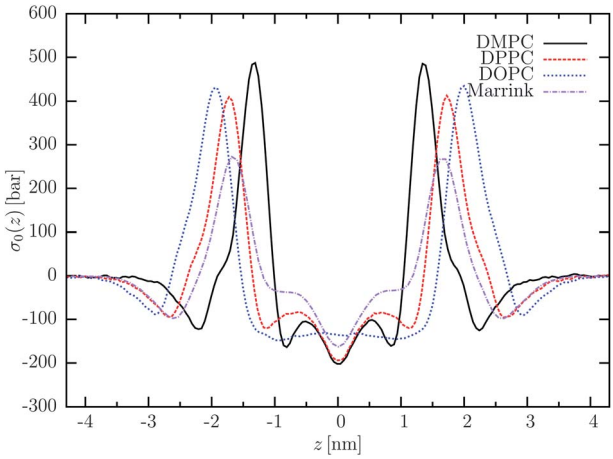

Fig. 2 The lateral stress profiles of DMPC (solid, black), DPPC (dashed, red) and DOPC (dotted, blue) bilayers of 256 lipids (DMPC and DOPC at 300 K, DPPC at 323 K). The stress profile by Marrink *et al.*[46] (DPPC, 512 lipids, 323 K) is shown as the purple and dash–dotted curve for comparison.

negative K_{0m} (eqn (10)), a positive value of $\bar{\kappa}$ means that the lamellar phase becomes unstable,[62] which contradicts the fact that both of these two PC lipids form perfectly stable bilayers—both experimentally and in simulation.

Eqn (8c) implies that $\bar{\kappa}_m/\kappa_m$ depends quadratically on z_0:

$$\frac{\bar{\kappa}_m}{\kappa_m} = \frac{\bar{\kappa}}{\kappa} + 2K_{0m}z_0 - \frac{\Sigma}{\kappa}z_0^2, \tag{16}$$

but using the actual values from Table 2 shows that the quadratic term is very small compared to the other two for reasonable values of z_0; hence the dependence is *de facto* linear. For each system one can thus estimate the elastic monolayer ratio,

Table 2 Spontaneous curvatures and elastic ratios of some MARTINI membranes using the stress profile method[a]

#	Lipid	$N_L\|\frac{4N_W}{N_L}$	T [K]	$\Sigma\left[\frac{mN}{m}\right]$	K_{0m} [nm^{-1}]	$\bar{\kappa}/\kappa$
1	DMPC	128|46	300	0.43 ± 0.09	−0.077 ± 0.001	−0.045 ± 0.004
2	DMPC	256|46	300	0.09 ± 0.08	−0.070 ± 0.001	−0.053 ± 0.003
3	DMPC	512|52	300	−0.17 ± 0.05	−0.067 ± 0.001	−0.061 ± 0.003
4	DMPC	256|79	300	0.02 ± 0.06	−0.063 ± 0.001	−0.074 ± 0.003
5	DPPC	256|42	300	0.08 ± 0.08	−0.141 ± 0.001	0.116 ± 0.004
6	DPPC	256|42	323	0.12 ± 0.08	−0.146 ± 0.001	0.135 ± 0.004
7	DOPC	256|41	300	0.14 ± 0.08	−0.246 ± 0.001	0.481 ± 0.004

[a] N_L is the number of lipids in the bilayer; N_W is the number of CG water molecules, which is equivalent to 4 real water molecules; T is the temperature; Σ is the zeroth moment of the bilayer stress profile, which equals the surface tension; K_{0m} is the lipid spontaneous curvature, calculated using eqn (8a), with $\kappa_m = \frac{1}{2}\kappa = 8.3 \times 10^{-20}$ J from Table 1; $\bar{\kappa}/\kappa$ is the bilayer elastic ratio. All error bars come from MC resampling of the original stress profiles, but probably underestimate the correlation corrections between the frames. Note that: 1) the same κ from DMPC is assumed for DPPC and DOPC; 2) MARTINI-DPPC membranes remain in the fluid phase at 300 K.[47]

which unfortunately depends on somewhat arbitrary assumptions about z_0 in the absence of an independent measurement of the neutral surface. For instance, in system 2, generously bracketing z_0 between (0.5 and 2.0) nm gives $\bar{\kappa}_m/\kappa_m$ in a range of (-0.12 to -0.33). While this covers a range of a factor of 3, it is still far off compared to our previously estimated and experimentally supported value $\bar{\kappa}_m/\kappa_m \approx -1$. If we wanted to achieve the latter value, we would have to pick $z_0 \approx 7$ nm, which is entirely implausible. In other words, no physically justifiable choice for z_0 can bring the stress-derived results for the elastic monolayer ratio in agreement with our measurement from the patch-closure method in Section 4.1.

To further investigate what affects the stress profile, systems with various geometries and simulation conditions were studied. First, to examine the size-dependence, systems 1–3 with various numbers of lipids are compared in Fig. 1. The three profiles qualitatively agree with each other, both in shape and in the positions of the extrema. Yet, a clear trend of decreasing magnitudes of extrema was observed as the system size was increased. This is most likely a consequence of the larger undulations in bigger systems, as explained above. However, for the present analysis it is the first and second moment of these profiles which matters and, as proved in Section 2.2.2, the undulation broadening does not affect the monolayer and bilayer moments for the sizes we have studied. Remaining differences likely stem from differences in hydration, a remaining tension in the 128 lipid system and possibly genuine finite size effects beyond trivial broadening. We subsequently chose a system size of 256 lipids to simultaneously remain efficient and reduce finite-size effects.

Second, a different hydration level was tested in system 4. The hydration ratio $4N_W/N_L$ was raised from 46 in system 2 to 79. Here, N_W is the number of CG water molecules, each representing 4 real water molecules in the MARTINI model. The stress profile of this more hydrated system did not differ noticeably from that of system 2, which indicates that the hydration level of system 2 suffices. While the first moment, and thus the spontaneous lipid curvature, hardly changed, the second moment and the elastic ratio differ by almost 50%, together with a greatly increased error. This is likely to be due to the increasing uncertainty of the stress profile tails in the bulk water region. The second moment is more sensitive to the value of $\sigma_0(z)$ far away from the reference plane because of its quadratic dependence on position z. To avoid such complications with the stress noise in the water region, we only integrated within $|z| \leq 4.5$ nm; however, then there is no need to have more than 41 to 45 (real) water molecules per lipid and so we subsequently restricted to this value.

Third, the effects of chain length and saturation were evaluated by simulating systems consisting of 256 DMPC, DPPC and DOPC lipids. Two changes are evident as the chain length increases: first, the stress profile widens, since the bilayer thickness increases (Fig. 2) and second, the hydrophobic regions of the stress profiles flatten; hence the position of the neutral surface becomes a bit more uncertain and with it the value of the monolayer elastic ratio also becomes uncertain. Note that the same bending modulus κ from the DMPC bilayer in Table 1 was assumed for the DPPC and DOPC systems. Thus, we can compare different lipid systems only qualitatively.

Regardless of the exact values, the measured spontaneous curvatures K_{0m} using the stress profile method seem to exhibit a systematic trend towards more negative values, as discussed at the beginning of this section. Although the same CG model is used, it is at present unclear why the current results on K_{0m} do not agree with previously reported[46] ones from a simulation of 512 DPPC.§

§ In our experience, the measured stress depends sensitively on the details of the simulation, which for many other observables do not greatly matter. For instance, we have observed a slight dependence of the stress profile on the coupling constants of the barostat (*e.g.*, $\tau_p = 3$ ps *vs.* $\tau_p = 0.2$ ps; results not shown). Such differences will be amplified when calculating the moments. We have not followed up these observations in detail, but would like to point out that any accurate and reproducible extraction of parameters from the stress profile would ultimately have to address these issues.

As can be seen from Fig. 2, apart from the reduction in the magnitudes due to the difference in the system size, there is also a minor variation in the profile shape around the hydrophobic region. One possible reason is the different methods adopted for the pressure tensor calculation. Instead of the 3-dimensional pressure field calculation described in Section 2.2, a slice-based method by Lindahl and Edholm[18] was used in the previous study.[46] On the other hand, our current results are in good agreement with another study by Ollila and Vattulainen,[80] who used an all-atom membrane model to investigate both K_{0m} and the elastic ratio.

5 Discussion

The curvature–elastic properties of a DMPC membrane were independently studied using the membrane patch-closure method and the stress profile method. While the results from the former semi-quantitatively follow expectations, the ones produced by the latter appear unphysical.

For the patch-closure method, the major contribution to the statistical error of $\bar{\kappa}$ stems from the uncertainty in the measurement of the bending modulus κ, since all other input parameters, such as the area per molecule and the edge tension, can be measured with comparatively high accuracy. From our simulations, even though the statistical error on κ seems moderate, the systematic error is probably larger ($\sim$10% if one compares the original result by Brandt *et al.*[53] and our measurements) and hard to quantify. Meanwhile, the values of κ measured in experiments also span over a fairly big range,[63] reminding us that accurately determining κ is still not quite trivial—both in simulations and in experiments.

Both the absolute value of the Gaussian modulus $\bar{\kappa}$ and the elastic ratio $\bar{\kappa}/\kappa$, when obtained by our patch-closure method, depend on the value of the bending modulus κ. To show this dependence, $\bar{\kappa}/\kappa$ as a function of κ is plotted in Fig. 3 (assuming always the same value for ξ). The definition of ξ in eqn (3) gives $\bar{\kappa}/\kappa = (\gamma R/\xi)/\kappa - 2$, which is shown as the solid curve. Assuming the relative error of the bending modulus σ_κ/κ we measured also applies to other κ values, the error on $\bar{\kappa}/\kappa$ can also be estimated from error propagation and is drawn as the grey region in the figure. Notice that if we take $\kappa < 8 \times 10^{-20}$ J, the elastic ratio becomes positive and thus unphysical, and yet such a bending rigidity is within the range of what has been measured experimentally, (5–15) $\times 10^{-20}$ J.[63] Of course, this merely illustrates how dangerous it is to mix values coming from very different sources. There is no reason to expect that the actual bending rigidity of MARTINI-DMPC exactly equals the experimental one and even a factor of only 2 (which is not bad given the experimental uncertainties) will, in this case, make a big difference. Notice that if we take the value of the bending rigidity as actually determined for MARTINI-DMPC, *i.e.* if we remain internally consistent, the elastic ratio agrees with the expectation.¶

Notice that the patch-closure method is computationally remarkably inexpensive. As can be read from Table 1, 60 runs for each initial configuration are sufficient to produce a ξ value that is more than accurate enough compared to all other parameters. Each single simulation contains roughly 75000 particles and can (currently) be simulated at about 200 ns per day using a cluster node with 8 CPUs. Although the membrane vesiculation time varies from tens of nanoseconds to a few microseconds, due to its probabilistic nature, on average 100 to 200 nanoseconds is enough to decide whether a given simulation leads to flattening or closure. Thus, all 400 simulations can be finished in a few months, given 6 to 8 cluster nodes. This estimated time can be further shortened if more computation resources are available, since

¶ One may then question the validity of the estimation previously made in section 4.1, which connected the measured bilayer elastic ratio to its monolayer counterpart. Yet, this was an estimation about the *geometry* of DMPC lipids, which the MARTINI model seems to reproduce well.[46]

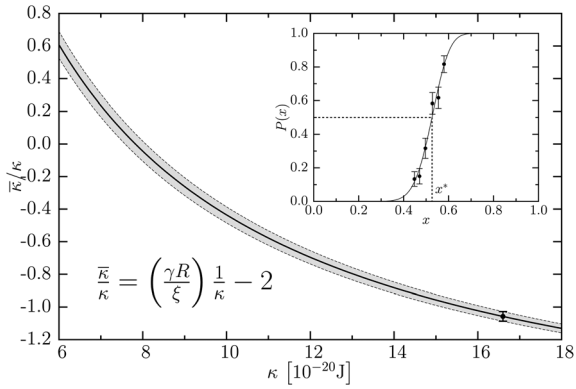

Fig. 3 The dependence of the elastic ratio $\bar{\kappa}/\kappa$ on the value of κ, shown as the solid curve. Simulation values of γ, R and ξ from Table 1 were used. The dashed lines above and below the solid line denote the error on $\bar{\kappa}/\kappa$, assuming the relative error σ_κ/κ is the same throughout the range of κ plotted. The inset shows the patch-closure probabilities P_{close} measured from simulations, as well as the fit to their analytical expression.

the procedure trivially parallelizes. At such costs, it should become affordable to exploit the versatility of the MARTINI model and examine more complex membrane systems, such as lipid–cholesterol mixtures, *e.g.* to study a conceivable tuning of the Gaussian curvature modules through the membrane composition.

Unfortunately, even though the stress profile method to calculate $\bar{\kappa}$ requires less simulation effort, the results it generates appear questionable. By applying essentially the same method, several attempts have been made in recent years to study the curvature elastic properties of a variety of lipid membranes, using either coarse-grained[46,81–83] or all-atom[79,80] lipid models. Some relevant results are collected in Table 3. Including our current results, most of the reported monolayer elastic ratios scatter within the range of 0 and −0.5. Despite the fact that such a range is compatible with the general requirement of $-1 < \bar{\kappa}_{\mathrm{m}}/\kappa_{\mathrm{m}} < 0$,[41] it is small in magnitude compared to the few available experimental measurements around −0.8 (see the summary of the available experimental and simulation results in ref. 36), which agree with our patch-closure method.

Two major possibilities can, in principle, lead to such a discrepancy: either the stress profile method itself is faulty, or the MARTINI model is unable to reproduce the correct curvature elasticity. In addition to the reasonable direct measurements of the spontaneous curvatures of several types of MARTINI lipids, including DPPC and DOPC,[46] other indirect studies also suggest that the real spontaneous curvatures of MARTINI lipids are not as strong as the stress profile method will make us believe. In a recent study on the curvature-inducing effects of membrane fusion peptides,[49] under comparable hydration conditions, MARTINI-DOPC lipids have been shown to prefer the lamellar phase to other lipids with high curvatures (*e.g.* the inverse hexagonal phase and single or double diamond phases, *etc.*), while DOPE will choose the opposite. Such observations agree well with the general experimental picture and the expectations derived from it over many years. Thus, it is likely that the MARTINI model is in fact able to provide realistic representations of lipid curvatures, thereby suggesting that the trouble lies with eqn (8, 9).

A few further comments should be made on the stress profile method. First of all, although most of the simulation models of biological membranes are able to reproduce the macroscopic membrane structure correctly, the stress profiles may be very sensitive to minute details in the force fields for the reason that the virial contribution to the pressure tensor is directly determined by the *local* interactions defined in the force field. Thus, one should not take the results from the stress profiles for

Table 3 Spontaneous curvatures and elastic ratios of common membranes using the stress profile method[a]

Lipid	Ref.	κ [10^{-20} J]	K_{0m} [nm^{-1}]	$\bar{\kappa}_m/\kappa_m$	$\bar{\kappa}/\kappa$
DMPC	CG[81]	9.0 ± 0.7	−0.018 ± 0.003	−0.49 ± 0.04	−0.49
	CG[82]	4.3 ± 0.1	+ 0.135 ± 0.002	−1.33 ± 0.04	−1.62
	CG	16.6 ± 0.5	−0.070 ± 0.001	−0.26 ± 0.07	−0.05
DPPC	AA[80]	5 ± 2	−0.22 ± 0.14	−0.22 ± 0.13	
	CG[46]	6...14	−0.02...−0.05		
	CG	(16.6 ± 0.5)	−0.146 ± 0.001	−0.36 ± 0.15	+0.14
DOPC	AA[80]	5 ± 2	−0.32 ± 0.22	−0.22 ± 0.18	
	CG[46]	6...14	−0.07...−0.15		
	CG[82]	12.3 ± 0.4	−0.087 ± 0.003	−0.45 ± 0.02	−0.23
	CG[83]	8.5...11.8	−0.06...−0.09	−0.33...−0.42	−0.13...−0.15
	CG	(16.6 ± 0.5)	−0.246 ± 0.001	−0.50 ± 0.25	+0.48

[a] References indicate the original study from which the data is quoted, with "CG" and "AA" meaning coarse-grained and all-atom models; κ is the bilayer bending modulus used to calculate the elastic properties, which is either from simulations (current study and ref. 81–83) or from experiments (ref. 46 and 80); K_{0m} is the lipid spontaneous curvature; $\bar{\kappa}_m/\kappa_m$ is the reported monolayer elastic ratio; $\bar{\kappa}/\kappa$ is the bilayer elastic ratio, calculated *via* eqn (10) whenever the position of the neutral surface z_0 is given. No error is listed for $\bar{\kappa}/\kappa$ due to the missing error of z_0. All values and corresponding error bars are either quoted or calculated based on the available data from the original source. Ref. 83 contains results for three different system sizes, thus the range is listed. Rows without references are from the current study, in which the bending rigidity κ of DMPC is used for all three lipid types and the error on the monolayer elastic ratio is estimated by shifting z_0 within a range of 0.5 nm around the global maximum in the stress profile.

granted even if the model has been proved useful when dealing with certain macroscopic problems. The greatly different elastic properties measured by Orsi *et al.* between two versions[81,82] of their CG models serve as a good example. With modifications to the earlier model, some of the important properties of lipid membranes, such as the dipole potential, were improved.[82] Yet, qualitative changes were observed in the measured spontaneous curvature and elastic ratio, which testify to the mercurial nature of the pressure calculation.

Secondly, if one decides to adopt the stress profile method to quantitatively study some membrane properties, one should note that systematic errors could potentially dominate the final results: in addition to the corresponding profile moments, the spontaneous curvature is affected by the value of the bending modulus, while the monolayer elastic ratio is affected by the position of the neutral surface. Both numbers are not trivially pinpointed, especially the latter. Also, despite the fact that the calculation of the bilayer elastic ratio does not depend on κ or z_0, it is highly sensitive to the water region in simulations as a result of the quadratic dependence on the normal position. In other words, the bilayer elastic ratio is substantially influenced by the profile tails.

Thirdly, our previously documented failure of the stress profile method to capture the elastic ratio could have been attributed to the use of a very simple lipid model.[36] Yet, using the more highly resolved MARTINI model does not lead to a better prediction based on $\sigma_0(z)$, even though, intriguingly, the error goes in the opposite direction: while the predicted elastic ratio of the simple lipid model was −1.7, and thus implausibly small, the values for MARTINI-DMPC, which hover around −0.05, are implausibly large. As we pointed out earlier,[36] it might not be the lack of local correlations in the highly coarse-grained Cooke model that is to blame, but the neglect of the local correlation inherent in the continuum theory that leads

to the stress profile formulas eqn (8, 9). Moreover, Oversteegen and Leermakers[85] have pointed out that the relationship between the stress profile moments and the elastic constants should contain additional thermodynamic derivatives, which the standard derivations neglect.

Stress profile calculations have been successfully used in many interesting studies, despite the caveats discussed by us. For instance, the effects of the incorporation of sterols on membrane mechanical properties were shown to be more complex than previously thought: sterols not only fluidize the gel phase and order the liquid phase, but also redistribute the stress along the bilayer.[86] Moreover, the free energy difference associated with the structural changes of the integral membrane proteins (*e.g.* the mechanosensitive channel, MscL[87]) caused by the pressure–volume work against the local bilayer stresses was studied in simulations.[79,80,88] Nevertheless, our results suggest that using the stress profile method to accurately determine the curvature elastic properties of biomembranes remains a concern.

Acknowledgements

We enjoyed stimulating discussions with Erik Brandt, Alex de Vries and Samuli Ollila. MH, MD and SJM are grateful for the hospitality of KITP, where part of this work was completed. This research was supported, in part, by the National Science Foundation under Grant No. NSF PHY11-25915 and CMMI-0941690.

References

1 H. Lodish, A. Berk, C. A. Kaiser, M. Krieger, M. P. Scott, A. Bretscher, H. Ploegh and P. Matsudaira, *Molecular Cell Biology*, W. H. Freeman, New York, 6th edn, 2007.
2 W. Helfrich, *Z. Naturforsch. C*, 1973, **28**, 693–703.
3 W. Helfrich, *Phys. Lett. A*, 1974, **50**, 115–116.
4 F. Brochard and J. F. Lennon, *J. Phys.*, 1975, **36**, 1035–1047.
5 F. Brochard, P.-G. de Gennes and P. Pfeuty, *J. Phys.*, 1976, **37**, 1099–1104.
6 M. B. Schneider, J. T. Jenkins and W. W. Webb, *Biophys. J.*, 1984, **45**, 891–899.
7 M. B. Schneider, J. T. Jenkins and W. W. Webb, *Biophys. J.*, 1984, **45**, 1457–1472.
8 J. F. Faucon, M. D. Mitov, P. Méléard, I. Bivas and P. Bothorel, *J. Phys.*, 1989, **50**, 2389–2414.
9 J. Henriksen, A. C. Rowat and J. H. Ipsen, *Eur. Biophys. J.*, 2004, **33**, 732–741.
10 Y. F. Liu and J. F. Nagle, *Phys. Rev. E: Stat., Nonlinear, Soft Matter Phys.*, 2004, **69**, 040901.
11 N. Chu, N. Kučerka, Y. F. Liu, S. Tristram-Nagle and J. F. Nagle, *Phys. Rev. E: Stat., Nonlinear, Soft Matter Phys.*, 2005, **71**, 041904.
12 S. Tristram-Nagle and J. F. Nagle, *Biophys. J.*, 2007, **93**, 2048–2055.
13 J. Pan, S. Tristram-Nagle, N. Kučerka and J. F. Nagle, *Biophys. J.*, 2008, **94**, 117–124.
14 L. Bo and R. E. Waugh, *Biophys. J.*, 1989, **55**, 509–517.
15 D. Cuvelier, I. Derényi, P. Bassereau and P. Nassoy, *Biophys. J.*, 2005, **88**, 2714–2726.
16 A. Tian and T. Baumgart, *Biophys. J.*, 2009, **96**, 2676–2688.
17 R. Goetz, G. Gompper and R. Lipowsky, *Phys. Rev. Lett.*, 1999, **82**, 221–224.
18 E. Lindahl and O. Edholm, *Biophys. J.*, 2000, **79**, 426–433.
19 G. Ayton and G. A. Voth, *Biophys. J.*, 2002, **83**, 3357–3370.
20 O. Farago, *J. Chem. Phys.*, 2003, **119**, 596–605.
21 S. J. Marrink, A. H. de Vries and A. E. Mark, *J. Phys. Chem. B*, 2004, **108**, 750–760.
22 Z.-J. Wang and D. Frenkel, *J. Chem. Phys.*, 2005, **123**, 154701.
23 I. R. Cooke, K. Kremer and M. Deserno, *Phys. Rev. E: Stat., Nonlinear, Soft Matter Phys.*, 2005, **72**, 011506.
24 R. Cooke and M. Deserno, *J. Chem. Phys.*, 2005, **123**, 224710.
25 G. Brannigan and F. L. H. Brown, *Biophys. J.*, 2006, **90**, 1501–1520.
26 Z.-J. Wang and M. Deserno, *J. Phys. Chem. B*, 2010, **114**, 11207–11220.
27 V. A. Harmandaris and M. Deserno, *J. Chem. Phys.*, 2006, **125**, 204905.
28 A. Arkhipov, Y. Yin and K. Schulten, *Biophys. J.*, 2008, **95**, 2806–2821.
29 S. Baoukina, S. J. Marrink and D. P. Tieleman, *Biophys. J.*, 2012, **102**, 1866–1871.
30 C. Taupin, M. Dvolaitzky and C. Sauterey, *Biochemistry*, 1975, **14**, 4771–4775.
31 D. V. Zhelev and D. Needham, *Biochim. Biophys. Acta, Biomembr.*, 1993, **1147**, 89–104.

32 I. Genco, A. Gliozzi, A. Relini, M. Robello and E. Scalas, *Biochim. Biophys. Acta, Biomembr.*, 1993, **1149**, 10–18.
33 E. Karatekin, O. Sandre, H. Guitouni, N. Borghi, P. H. Puech and F. Brochard-Wyart, *Biophys. J.*, 2003, **84**, 1734–1749.
34 E. Kreyszig, *Differential Geometry*, Dover, New York, 1991.
35 M. do Carmo, *Differential Geometry of Curves and Surfaces*, Prentice Hall, Englewood Cliffs, NJ, 1976.
36 M. Hu, J. J. Briguglio and M. Deserno, *Biophys. J.*, 2012, **102**, 1403–1410.
37 D. P. Siegel and M. M. Kozlov, *Biophys. J.*, 2004, **87**, 366–374.
38 D. P. Siegel, *Biophys. J.*, 2006, **91**, 608–618.
39 D. P. Siegel, *Biophys. J.*, 2008, **95**, 5200–5215.
40 S. Lorenzen, R.-M. Servuss and W. Helfrich, *Biophys. J.*, 1986, **50**, 565–572.
41 R. H. Templer, B. J. Khoo and J. M. Seddon, *Langmuir*, 1998, **14**, 7427–7434.
42 S. Semrau, T. Idema, L. Holtzer, T. Schmidt and C. Storm, *Phys. Rev. Lett.*, 2008, **100**, 088101.
43 T. Baumgart, S. Das, W. W. Webb and J. T. Jenkins, *Biophys. J.*, 2005, **89**, 1067–1080.
44 G. Brannigan, P. F. Philips and F. L. H. Brown, *Phys. Rev. E: Stat., Nonlinear, Soft Matter Phys.*, 2005, **72**, 011915.
45 G. Brannigan and F. L. H. Brown, *Biophys. J.*, 2007, **92**, 864–876.
46 S. J. Marrink, H. J. Risselada, S. Yefimov, D. P. Tieleman and A. H. de Vries, *J. Phys. Chem. B*, 2007, **111**, 7812–7824.
47 S. J. Marrink, J. Risselada and A. E. Mark, *Chem. Phys. Lipids*, 2005, **135**, 223–244.
48 Y. G. Smirnova, S. J. Marrink, R. Lipowsky and V. Knecht, *J. Am. Chem. Soc.*, 2010, **132**, 6710–6718.
49 M. Fuhrmans and S. J. Marrink, *J. Am. Chem. Soc.*, 2012, **134**, 1543–1552.
50 H. J. Risselada and S. J. Marrink, *Proc. Natl. Acad. Sci. U. S. A.*, 2008, **105**, 17367–17372.
51 H. J. Risselada, S. J. Marrink and M. Müller, *Phys. Rev. Lett.*, 2011, **106**, 148102.
52 M. Louhivuori, H. J. Risselada, E. Van Der Giessen and S. J. Marrink, *Proc. Natl. Acad. Sci. U. S. A.*, 2010, **107**, 19856–19860.
53 E. G. Brandt, A. R. Braun, J. N. Sachs, J. F. Nagle and O. Edholm, *Biophys. J.*, 2011, **100**, 2104–2111.
54 P. Fromherz, *Chem. Phys. Lett.*, 1983, **94**, 259–266.
55 N. G. van Kampen, *Stochastic Processes in Physics and Chemistry*, Elsevier, Amsterdam, 3rd edn, 2007.
56 H. Noguchi and G. Gompper, *J. Chem. Phys.*, 2006, **125**, 164908.
57 W. Shinoda, T. Nakamura and S. O. Nielsen, *Soft Matter*, 2011, **7**, 9012–9020.
58 W. Helfrich, *Physics of Defects*, North-Holland, Amsterdam, 1981, pp. 715–755.
59 I. Szleifer, D. Kramer, A. Ben-Shaul, W. M. Gelbart and S. A. Safran, *J. Chem. Phys.*, 1990, **92**, 6800–6817.
60 G. Gompper and S. Klein, *J. Phys. II*, 1992, **2**, 1725–1744.
61 G. Gompper and S. Zschocke, *Phys. Rev. A: At., Mol., Opt. Phys.*, 1992, **46**, 4836–4851.
62 W. Helfrich, *J. Phys.: Condens. Matter*, 1994, **6**, A79–A92.
63 D. Marsh, *Chem. Phys. Lipids*, 2006, **144**, 146–159.
64 B. Hess, C. Kutzner, D. van der Spoel and E. Lindahl, *J. Chem. Theory Comput.*, 2008, **4**, 435–447.
65 W. F. Van Gunsteren and H. J. C. Berendsen, *Mol. Simul.*, 1988, **1**, 173–185.
66 H. J. C. Berendsen, J. P. M. Postma, W. F. van Gunsteren, A. DiNola and J. R. Haak, *J. Chem. Phys.*, 1984, **81**, 3684–3690.
67 H. J. Risselada, A. E. Mark and S. J. Marrink, *J. Phys. Chem. B*, 2008, **112**, 7438–7447.
68 N. Theodorou, Doros and U. W. Suter, *Macromolecules*, 1985, **18**, 1206–1214.
69 O. H. S. Ollila, H. Risselada, M. Louhivuori, E. Lindahl, I. Vattulainen and S. J. Marrink, *Phys. Rev. Lett.*, 2009, **102**, 078101.
70 W. H. Press, S. A. Teukolsky, W. T. Vetterling and B. P. Flannery, *Numerical Recipes*, Cambridge University Press, New York, 3rd edn, 2007.
71 N. Kučerka, Y. Liu, N. Chu, H. I. Petrache, S. Tristram-Nagle and J. F. Nagle, *Biophys. J.*, 2005, **88**, 2626–2637.
72 T. V. Tolpekina, W. K. den Otter and W. J. Briels, *J. Chem. Phys.*, 2004, **121**, 8014–8020.
73 J. Wohlert, W. K. den Otter, O. Edholm and W. J. Briels, *J. Chem. Phys.*, 2006, **124**, 154905.
74 F. Y. Jiang, Y. Bouret and J. T. Kindt, *Biophys. J.*, 2004, **87**, 182–192.
75 Z.-J. Wang and M. Deserno, *New J. Phys.*, 2010, **12**, 095004.
76 L. Chernomordik, M. Kozlov, G. Melikyan, I. Abidor, V. Markin and Y. Chizmadzhev, *Biochim. Biophys. Acta, Biomembr.*, 1985, **812**, 643–655.
77 M. C. Watson, E. S. Penev, P. M. Welch and F. L. H. Brown, *J. Chem. Phys.*, 2011, **135**, 244701–22.
78 D. Marsh, *Biophys. J.*, 2007, **93**, 3884–3899.

79 O. H. S. Ollila, T. Róg, M. Karttunen and I. Vattulainen, *J. Struct. Biol.*, 2007, **159**, 311–323.
80 O. H. S. Ollila and I. Vattulainen, *Molecular Simulations and Biomembranes*, Royal Society of Chemistry, Cambridge, 2010, pp. 26–55.
81 M. Orsi, D. Y. Haubertin, W. E. Sanderson and J. W. Essex, *J. Phys. Chem. B*, 2008, **112**, 802–815.
82 M. Orsi, J. Michel and J. W. Essex, *J. Phys.: Condens. Matter*, 2010, **22**, 155106.
83 M. Orsi and J. W. Essex, *PLoS One*, 2011, **6**, e28637.
84 J. A. Szule, N. L. Fuller and R. Peter Rand, *Biophys. J.*, 2002, **83**, 977–984.
85 S. M. Oversteegen and F. A. M. Leermakers, *Phys. Rev. E: Stat. Phys., Plasmas, Fluids, Relat. Interdiscip. Top.*, 2000, **62**, 8453–8461.
86 J. M. Vanegas, M. L. Longo and R. Faller, *J. Am. Chem. Soc.*, 2011, **133**, 3720–3723.
87 O. H. S. Ollila, M. Louhivuori, S. J. Marrink and I. Vattulainen, *Biophys. J.*, 2011, **100**, 1651–1659.
88 J. Gullingsrud and K. Schulten, *Biophys. J.*, 2004, **86**, 3496–3509.

